RESEARCH ARTICLE

IDACC: Image Dehazing Avoiding Color Cast Using a Novel Atmospheric Scattering Model

ZHIWEI LI[1,2], XINJIE XIAO[2], AND NANNAN ZHANG[2]
[1]Shanghai Technology and Innovation Vocational College, Shanghai 201620, China
[2]College of Information Science and Technology, Donghua University, Shanghai 201620, China

Corresponding author: Zhiwei Li (lzw0130@126.com)

ABSTRACT Images captured in hazy scenes exhibit severe degradation. Various dehazing methods have been proposed recently. However, most of them have the drawback of color cast in the dehazing results. To solve this problem, we proposed an image dehazing algorithm called IDACC that avoids color cast by using a novel atmospheric scattering model (NASM). The NASM is obtained by introducing a scattering compensation coefficient into the atmospheric light term of the traditional atmospheric scattering model (ASM). The scattering compensation coefficient effectively suppresses the color cast caused by the atmospheric light term. Moreover, we designed a global information search (GIS) strategy based on the minimum value channel to facilitate the calculation of the transmission map. Extensive experiments show that IDACC achieves image dehazing and effectively avoids color cast. Note that the IDACC algorithm does not require to consume time in dataset collection and model training. Furthermore, IDACC needs to only input a hazy image and can directly output a haze-free image. Besides, our method shows excellent performance both quantitatively and qualitatively compared with state-of-the-art (SOTA) methods.

INDEX TERMS Image dehazing, color cast, scattering compensation coefficient, atmospheric scattering model.

I. INTRODUCTION

Haze is a natural phenomenon caused by suspended particles scattering and absorbing light, such as atmospheric dust, smoke, and other solid particles. Haze results in images with a color cast, low contrast, and low clarity. The color cast phenomenon makes the image colors not match the colors of the real scene. This phenomenon has serious impacts on computer vision systems that rely on clear images [1], such as object detection [2], [3], [4], image classification [5], image understanding [6], [7] and segmentation [8]. Therefore, designing effective image dehazing methods that eliminate color casts is urgently required.

Traditional image dehazing methods use the traditional atmospheric scattering model (ASM) [9] to remove haze.

The associate editor coordinating the review of this manuscript and approving it for publication was Qilian Liang.

However, there are two main difficulties in image dehazing using the ASM, which include the estimation of atmospheric light A and transmission map t. Recently, various methods, such as prior-based methods [10], [11], [12], [13], [14], have been proposed to resolve the aforementioned difficulties. Although these methods for image dehazing all achieved significant visual improvements, there are still some restrictive weaknesses existing. A conspicuous limitation is that the quality of the dehazed image depends on whether the real scene is in agreement with the prior knowledge. In other words, it will produce undesirable results when the real scene is not in agreement with the prior knowledge, such as color cast in dehazing results. For example, although the dark channel prior [12] has been proposed based on numerous observations, it failed to accurately obtain A and t of the traditional ASM, resulting in dehazed images with a color cast, darkness, and halo. Non-local prior [14]

relies on the assumption that the color of haze-free images comprises several hundred different color approximations. This method achieves favorable dehazing results; however, it is not effective for outdoor dehazing and introduces color cast because it involves postprocessing operations to improve contrast.

Thus, various methods have been proposed to further address these drawbacks and reduce the dependence on prior knowledge [15], [16], [17], [18], [19]. Although they achieved remarkable results, color casts still exist in dehazing results. To completely mitigate the problems caused by prior knowledge, deep learning techniques have been introduced for image dehazing [20], [21], [22], [23], [24]. While learning-based methods have good dehazing performance, they consume a considerable amount of time in collecting dataset and training the network and can introduce color casts in dehazing results. For example, Qu et al. [25] and Chen et al. [26] adopted a hazy-to-clear image translation strategy, which does not depend on ASM. These methods achieve good visual results, but the dehazing results have color casts and low brightness. The present methods indeed produce satisfactory visual outputs. Nonetheless, the dehazing techniques introduce color imbalances and reduced brightness levels into the dehazed images. Such deviations have negative implications on the efficacy of subsequent tasks that inherently demand pristine image data, including applications in aerial imaging and environmental monitoring. These inherent drawbacks compromise the precision with which computational algorithms can effectively identify and analyze the intricate details contained within the dehazed images.

In this study, we propose a novel atmospheric scattering model (NASM), which introduces a scattering compensation coefficient into the atmospheric light term of the traditional ASM. The scattering compensation coefficient effectively suppresses the color cast (see section III for specific details). Furthermore, we designed an IDACC algorithm using the NASM. Next, we designed a global information search (GIS) strategy based on the minimum value channel to facilitate the calculation of the transmission map (see section IV for specific details). Moreover, extensive experiments have shown that the proposed method achieves excellent performance in both quantitative and qualitative comparisons (see section V for analysis and discussion). Our IDACC algorithm achieved the best results in synthetic datasets and real-world scene images compared with state-of-the-art (SOTA) dehazing methods because NASM better describes the imaging process of hazy images.

Unlike learning-based and prior-based dehazing methods, our method efficiently avoids color cast. Moreover, the IDACC algorithm neither requires prior knowledge and nor does it consume time in dataset collection or model training. Additionally, it avoids color over-saturation and halo in recovered images. In brief, IDACC can achieve image dehazing and effectively avoid color cast.

Our major contributions are as follows:
- An novel atmospheric scattering model (NASM) is designed, which showcases its effectiveness in overcoming color cast issues within images after the dehazing process. Here, the NASM was obtained by introducing a scattering compensation coefficient into the atmospheric light term of the traditional ASM.
- The IDACC algorithm is developed for image dehazing and to avoid color cast. Additionally, GIS was designed based on the minimum value channel to estimate the transmission map.
- We experimentally validated the proposed method on comprehensive hazy datasets. The results demonstrate the notable improvement regarding color cast and dehazing performance.

II. RELATED WORK
We briefly introduce some typical image dehazing methods, including prior-based and learning-based methods.

A. PRIOR-BASED IMAGE DEHAZING METHODS
Prior-based methods use prior knowledge to estimate two unknown parameters, the transmission map t and atmospheric light A. Then, ASM is used to remove haze. The difference between these prior-based methods is that they employ different methods to estimate both unknown parameters. For example, the dehazing method for maximizing an image's local contrast [11] is based on two observations and solves the limitation associated with previous methods that several images of one scene are required. Similarly, He et al. [12] proposed the dark channel prior based on numerous observations. However, their method fails in white or bright scenes. Zhu et al. [13] estimated t by restoring scene depth information using color attenuation prior. Berman et al. [14] assumed that the color of haze-free images comprises several hundred different color approximations and proposed a new non-local prior algorithm. Although these methods have made great progress in image dehazing, the results of dehazed images still contain color cast and haze residue because prior knowledge is not universally applicable.

B. LEARNING-BASED IMAGE DEHAZING METHODS
Recently, neural networks have been introduced into image dehazing. For example, previous works [20], [21], [22] focused on using deep learning methods to directly estimate both unknown parameters A and t for image dehazing. Although these methods solved the problem of relying on prior knowledge, they posed some problems due to incorrect estimation, such as color cast, detail loss, and artifact. The end-to-end methods [25], [26] adopted a haze-to-clear image translation strategy, which uses learning methods to identify potential connections between images and achieve haze removal without using ASM. Wu et al. [24] proposed a contrastive learning method for image dehazing, which leverages information from negative and positive images. Although these methods achieved satisfactory dehazing
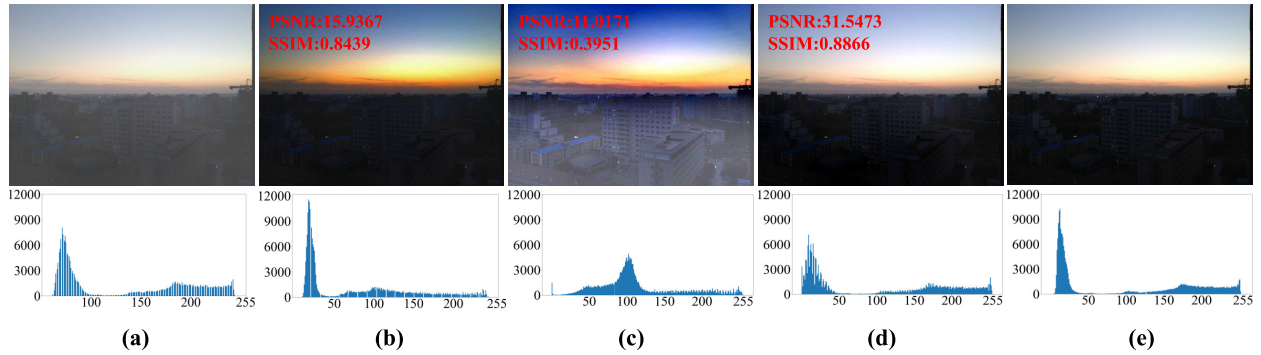
FIGURE 1. The first row indicates the dehazing results of different methods. The second row represents the histogram corresponding to the dehazing results. (a) Hazy image; (b) DCP; (c) IDE; (d) Proposed method; (e) Ground-truth.

results, they require considerable time to collect datasets and train models. Li et al. [23] proposed an unsupervised dehazing method called ZID, which does not require time for model training. However, ZID requires time to transform a haze image into a haze-free one and has a color cast in some dehazing results. Xiao et al. [27] proposed a self-supervised zero-shot dehazing network based on dark channel prior, which needs many iterations to obtain the dehazed image. Despite the learning-based methods improving the quality of the recovered image, they posed some problems, such as color cast, incomplete or excessive dehazing, loss of details, and so on.

In this study, we employ the NASM to design an IDACC algorithm that achieves hazy image dehazing and effectively avoids the occurrence of color cast. It is noted that the IDACC algorithm does not require hazy and clean image pairs for training compared to learning-based methods. Consequently, it eliminates the tedious work of dataset collection and does not require extensive time for model training. Moreover, our method only needs a hazy image input and it can directly output a high-quality haze-free image.

III. NOVEL ATMOSPHERIC SCATTERING MODEL

The formation process of the haze image can be described using the traditional ASM. From [9], [15], [16], and [28], we can obtain the mathematical expression of the traditional ASM as follows

$$Z_c(x) = N_c(x) \cdot t(x) + A_c \cdot (1 - t(x)), \tag{1}$$

where $c \in \{r, g, b\}$ is a color channel index, $Z_c(x)$ is a hazy image captured in the hazy scene, $N_c(x)$ is a haze-free image, A_c and $t(x)$ denote the atmospheric light and transmission map, respectively.

Furthermore, from [29], the traditional ASM can also be expressed as another mathematical expression

$$Z_c(x) = A_c(x) \cdot \rho(x) \cdot t(x) + A_c \cdot (1 - t(x)), \tag{2}$$

Obviously, $A_c(x) \cdot \rho(x) = N_c(x)$, $\rho(x)$ is the scene albedo.

The first term in Eq. (2) is called the direct attenuation term, representing the scene radiation and its attenuation in the medium. The second term is called the atmospheric light

term, representing the scattering of the ambient light through the atmospheric particles, and this term causes the color cast of the image. When the solid particles suspended in space are homogeneously distributed, the transmission map is defined by the mathematical expression as follows

$$t(x) = e^{-\beta \cdot d(x)}, \tag{3}$$

where β is the attenuation coefficient of the atmosphere and $d(x)$ is the scene depth at pixel x.

As previously described, prior-based dehazing methods can cause some problems. For example, non-local image dehazing [14] can cause color cast due to the use of the postprocessing operation for enhancing the contrast. The dehazing results of the dark channel prior [12] are dark and easily fail in white or bright scenes, leading to color cast and halo in the sky area. To address the dark problem of dehazing results, IDE [19] introduced the light absorption coefficient into the traditional ASM for image dehazing. Although this method effectively solves the low bright problem, image dehazing results are over bright and have color casts.

An analysis of previous descriptions revealed that the reason for the color cast is because of ignoring the scattering phenomenon of ambient light caused by the atmospheric light term in ASM. In the presence of haze, the proportion of light transmitted through the atmosphere decreases, leading to an overall decrease in image brightness. This phenomenon adversely affects both the contrast and color balance of the image. Therefore, we introduced a new scattering compensation coefficient $s(x) \in (0, 1]$ into the atmospheric light term of the traditional ASM to obtain NASM. This adjustment mitigates the the detrimental effects of atmospheric light, alleviating the issue of over-brightness in the dehazed images. It contributes to the preservation of overall image contrast and reduces the perception of color cast. The mathematical representation of NASM is different from the traditional ASM and NASM can be mathematically expressed as follows

$$Z_c(x) = N_c(x) \cdot t(x) + s(x) \cdot A_c \cdot (1 - t(x)), \tag{4}$$

Furthermore, we can obtain the following

$$Z_c(x) = A_c \cdot \rho(x) \cdot t(x) + s(x) \cdot A_c \cdot (1 - t(x)), \tag{5}$$

With increased scene depth, the atmospheric light term $A_c \cdot (1 - t(x))$ of the ASM leads to various degrees of color cast in dehazed images [30]. To eliminate color cast, we introduced a scattering compensation coefficient $s(x) \in (0, 1]$, where the atmospheric light term becomes $s(x) \cdot A_c \cdot (1 - t(x))$, thus weakening the scattering phenomenon of the atmospheric light term. Fig. 1 shows that from the macroscopic view and histogram distribution, introducing the scattering compensation coefficient suppresses the color cast phenomenon in image dehazing (specific experimental proofs are provided in section V).

Various scene depths will influence dehazed images differently [30]. As scene depth increases, the probability of encountering problems like color distortion and decreased brightness in dehazed images also rises. To alleviate these issues, drawing from experimental knowledge, the mathematical expression for the scattering compensation coefficient is presented as follows

$$s(x) = \frac{d(x)}{\max(d)},\quad (6)$$

Using Eq. (3), we can calculate

$$d(x) = -\frac{\ln(t(x))}{\beta},\quad (7)$$

$$\max(d) = -\frac{\ln(t_{min})}{\beta},\quad (8)$$

Combining Eqs. (6), (7), and (8), we know that

$$s(x) = \frac{\ln(t(x))}{\ln(t_{min})},\quad (9)$$

Similarly, combining Eqs. (5) and (9), we obtain NASM as follows

$$Z_c(x) = A_c \cdot \rho(x) \cdot t(x) + \frac{\ln(t(x))}{\ln(t_{min})} \cdot A_c \cdot (1 - t(x)),\quad (10)$$

NASM plays an essential role in image dehazing. We designed an IDACC algorithm using NASM in section IV. NASM guarantee that IDACC algorithm achieves hazy image dehazing and efficiently avoids color cast.

IV. THE PROPOSED IDACC USING NASM

We proposed an IDACC algorithm in which image dehazing and avoiding color cast using NASM. Furthermore, we designed a GIS strategy based on the minimum value channel to estimate the transmission map. Our method is divided into three steps. The flowchart of the IDACC algorithm can be seen in Fig. 2. First, from the methods in [16] and [17], we estimated the atmospheric light A. Second, we obtained the minimum value channel of the image and found the coarse transmission map using GIS based on the minimum value channel. Then, we obtained the refined transmission map t by guided filtering. Third, the derived A and t are introduced into the NASM for hazy image dehazing. Here, we mainly introduced these last two steps.
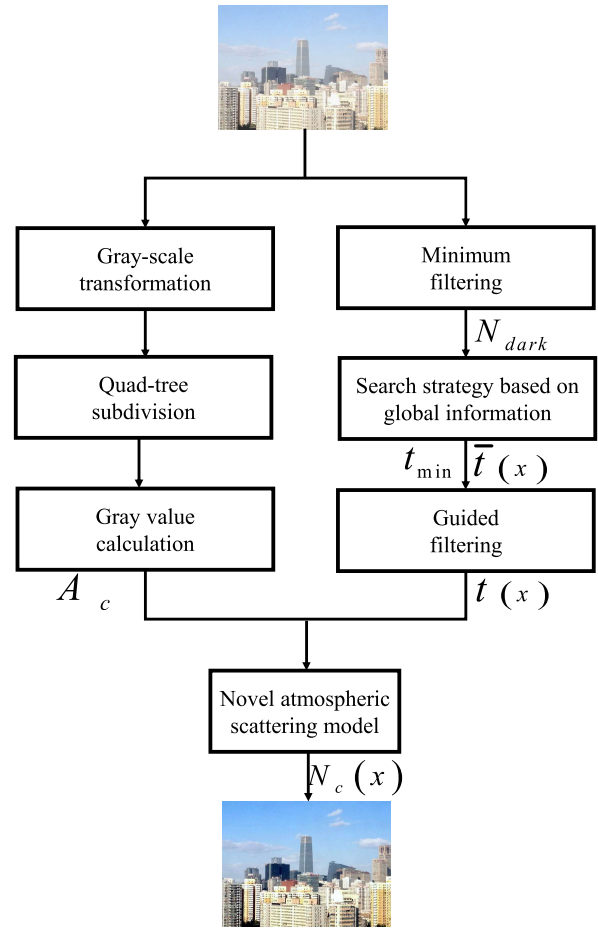

FIGURE 2. Flowchart of the proposed method.

A. ESTIMATION OF THE TRANSMISSION MAP

We divided the inputted hazy image into multiple local patches and considered each local patch as a small scene, denoted as follows

$$\overline{Z}_c(x) = A_m \cdot \rho(x) \cdot \bar{t}(x) + \frac{\ln(\bar{t}(x))}{\ln(t_{min})} \cdot A_m \cdot (1 - \bar{t}(x)),\quad (11)$$

Eq. (11) contains four unknown parameters A_m, $\rho(x)$, $\bar{t}(x)$, and t_{min}. A_m is the average of the three atmospheric light channels. $\bar{t}(x)$ is the transmission map of the local patch. To find $\bar{t}(x)$, the remaining three parameters must first be identified, where A_c can be easily found using the quad-tree method [16], [17], after which we can obtain A_m. According to previous studies [15], [19], and [31], we approximated $\rho(x) = \frac{1}{2}$. Now, combining Eqs. (11), we obtain the following

$$\overline{Z}_c(x) = \frac{1}{2} \cdot A_m \cdot \bar{t}(x) + \frac{\ln(\bar{t}(x))}{\ln(t_{min})} \cdot A_m \cdot (1 - \bar{t}(x)),\quad (12)$$

Eq. (12) contains a logarithmic function, which is more difficult to solve. Thus, we applied the fitting operation to simplify the calculation process. Therefore, from [19], we know that

$$\ln(\bar{t}(x)) \approx g(\bar{t}(x)) = \frac{n_1}{n_2 + \bar{t}(x)},\quad (13)$$

where $n_1 = -0.397$, $n_2 = 0.07747$ the logarithmic and rational functions have the best fit [19]. By substituting Eq. (13) into Eq. (12), we obtain the following

$$\overline{Z_c}(x) = \frac{n_1 \cdot A_m \cdot (1 - \bar{t}(x))}{(n_2 + \bar{t}(x)) \cdot \ln(t_{min})} + \frac{A_m}{2} \cdot \bar{t}(x), \qquad (14)$$

Furthermore, by simplification, we get

$$\left[\overline{Z_c}(x) \cdot \ln(t_{min}) - \frac{A_m}{2} \cdot n_2 \cdot \ln(t_{min}) + A_m \cdot n_1 \right] \cdot \bar{t}(x)$$
$$- \frac{A_m}{2} \cdot \ln(t_{min}) \cdot (\bar{t}(x))^2 + \overline{Z_c}(x) \cdot n_2 \cdot \ln(t_{min})$$
$$- A_m \cdot n_1 = 0, \qquad (15)$$

Note that Eq. (15) is a quadratic equation, which can be expressed as follows for more visualization

$$\alpha_1 \cdot (\bar{t}(x))^2 + \alpha_2 \cdot \bar{t}(x) + \alpha_3 = 0, \qquad (16)$$

where

$$\begin{cases} \alpha_1 &= -\frac{A_m}{2} \cdot \ln(t_{min}) \\ \alpha_2 &= \overline{Z_c}(x) \cdot \ln(t_{min}) - \frac{A_m}{2} \cdot n_2 \cdot \ln(t_{min}) + A_m \cdot n_1 \\ \alpha_3 &= \overline{Z_c}(x) \cdot n_2 \cdot \ln(t_{min}) - A_m \cdot n_1, \end{cases}$$
$$(17)$$

By solving quadratic equations (in the process of solving, we take positive values and ignore negative ones [19]), we can identify the unrefined transmission map. The expression for the solution is as follows

$$\bar{t}(x) = \frac{-\alpha_2 \pm \sqrt{(\alpha_2)^2 - 4 \cdot \alpha_1 \cdot \alpha_3}}{2 \cdot \alpha_1}, \qquad (18)$$

In the preceding description, we found A_c and $\rho(x)$. In Eq. (15), there are only two unknown parameters t_{min} and $\bar{t}(x)$. To find $\bar{t}(x)$, first, we find t_{min}. For finding t_{min}, we need to find the minimum value channel [12] of the input hazy image, which is given by

$$N_{dark}(x) = \min_{y \in P(x)} \left(\min_{c \in \{r,g,b\}} N_c(y) \right), \qquad (19)$$

where $P(x)$ is a local patch. After obtaining the minimum value channel $N_{dark}(x)$, from Eq. (12), we use GIS [19] based on $N_{dark}(x)$ to find t_{min}. Mathematically, this search strategy can be expressed as follows

$$t_{min} = GIS \Big\{ A_c, A_m, Z_c(x), N_c(x), N_{dark}(x), \rho(x),$$
$$n_1, n_2, H, W \Big\}, \qquad (20)$$

where H and W denote the image size. We use the golden section method in this search strategy to find t_{min}; then, $\bar{t}(x)$ can be easily obtained.

Furthermore, we use guided filtering [32] to refine and obtain the refined transmission map. This makes the image smoothly transition while maintaining edge information of the image.

B. HAZE REMOVAL
Combining Eqs. (4), (9), and (13), we obtain the following

$$Z_c(x) = N_c(x) \cdot t(x) + \frac{n_1 \cdot A_c \cdot (1 - t(x))}{(n_2 + \bar{t}(x)) \cdot \ln(t_{min})}, \qquad (21)$$

Furthermore, we obtain that

$$N_c(x) = \left\{ Z_c(x) - \frac{A_c \cdot n_1 \cdot [1 - t(x)]}{[n_2 + t(x)] \cdot \ln(t_{min})} \right\} \cdot \frac{1}{t(x)}, \qquad (22)$$

As A_c, $t(x)$ has been obtained, and n_1, n_2 are known, then we can use Eq. (22) for image dehazing. The experiments will demonstrate that the dehazed images closely resemble real-world scenes as perceived by the human eye, and the resulting recovery effectively eliminates color cast. To enhance clarity, this paper delineates the step-by-step process of the proposed IDACC method in Algorithm 1.

Algorithm 1 Proposed IDACC

Input: Hazy image $Z_c(x)$
Output: Dehazed image $N_c(x)$
Procedure:
1. Estimate the atmospheric light A using methods from [16,17].
2. Obtain the minimum value channel map $N_{dark}(x)$ from $Z_c(x)$.
3. For each local patch in $Z_c(x)$:
   3.1 Compute A_m, the average of A's RGB channels.
   3.2 Set $\rho(x) = \frac{1}{2}$ based on literature [15], [19], and [31].
   3.3 Use the minimum value channel map $N_{dark}(x)$ and GIS to find the coarse transmission map $\bar{t}(x)$.
4. Apply guided filtering to refine $\bar{t}(x)$ into the final transmission map $t(x)$.
5. Compute dehazed image $N_c(x)$ using Eq. (13) and (22).
Return $N_c(x)$.

V. EXPERIMENTS
We employed the IDACC algorithm based on NASM to achieve a perfect haze removal. Furthermore, we compared IDACC with eight existing methods. These methods encompass ASM-based approaches, such as DCP(2010) [12], IDE(2021) [19], DDAP(2021) [33] and SLP(2023) [34], and learning-based methods, including DehazeNet(2016) [21], AOD-Net(2017) [20], EPDN(2019) [25], TCN(2021) [35] and USID-Net(2022) [36]. All methods were implemented using HP laptops with an Intel(R) Core (TM) i5-6300 HQ CPU@ 2.30 GHz 8.00 GB RAM. The proposed IDACC, IDE [19], DDAP [33], SLP [34] and DehazeNet [21] were implemented in MATLAB2016B, while DCP [12], AOD-Net [20], EPDN [25], TCN [35], and USID-Net [36] were implemented in Python 3.6.

A. EXPERIMENTAL SETTINGS
1) DATASETS
In our experiments, we used the SOTS and HSTS, sourced from RESIDE [37] as the synthetic dataset.

FIGURE 3. Comparison with SOTA on histogram similarity. In the red box, the column chart shows the mean of the histogram similarity in the SOTS dataset. The yellow box shows the comparison of our results with SOTA on M1 dehazing, where Im1 is a hazy image from the SOTS dataset.
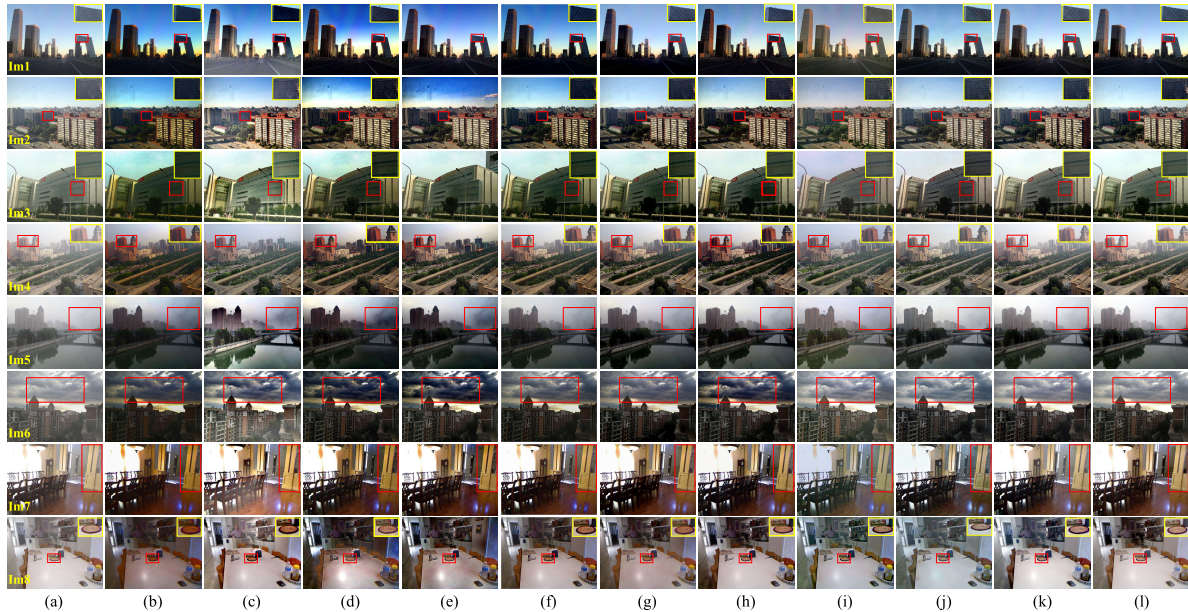
FIGURE 4. Qualitative comparison on SOTS. (a) Hazy-Image; (b) DCP [12]; (c) IDE [19]; (d) DDAP [33] (e) SLP [34](f) AOD-Net [20]; (g) DehazeNet [21]; (h) EPDN [25]; (i) TCN [35]; (j) USID-Net [36]; (k) Proposed method; (l) Ground-truth.

The SOTS dataset contains 1000 images, from which 150 images were randomly selected for the experiment. The HSTS dataset contains synthetic and real-world images. Moreover, we used I-HAZE [38] (35 hazy images) and O-HAZE [39] (45 hazy images) as the real-world datasets. Furthermore, we collected some hazy images from the Internet.

2) EVALUATION METRICS
We used peak signal-to-noise ratio (PSNR) and structural similarity (SSIM) to evaluate image quality. The higher the score of both metrics, the better the recovered image quality.

B. PROOF OF EFFECTIVENESS IN AVOIDING COLOR CAST
Histograms can describe the global distribution of colors in an image. To prove that our method effectively avoids color cast, we calculated the histogram similarity between the haze-free images obtained from different dehazing methods and the ground-truth images using the following mathematical equation

$$\begin{cases} C_j & = \dfrac{1}{N} \sum_{i=0}^{N} \left(1 - \dfrac{|g_i - s_i|}{Max\,(g_i, s_i)}\right) \\ C_m & = \dfrac{1}{Z} \sum_{j=1}^{Z} C_j, \end{cases} \tag{23}$$
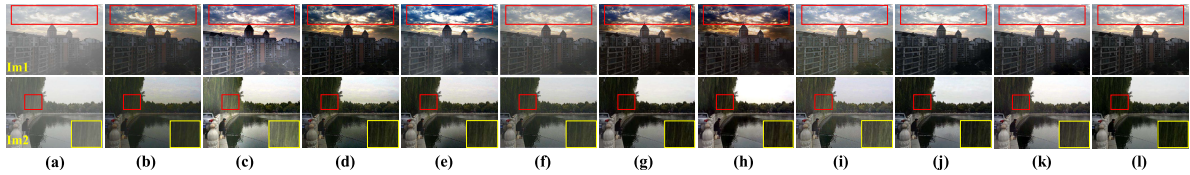
FIGURE 5. Qualitative comparison on HSTS. (a) Hazy-Image; (b) DCP [12]; (c) IDE [19]; (d) DDAP [33] (e) SLP [34](f) AOD-Net [20]; (g) DehazeNet [21]; (h) EPDN [25]; (i) TCN [35]; (j) USID-Net [36]; (k) Proposed method; (l) Ground-truth.
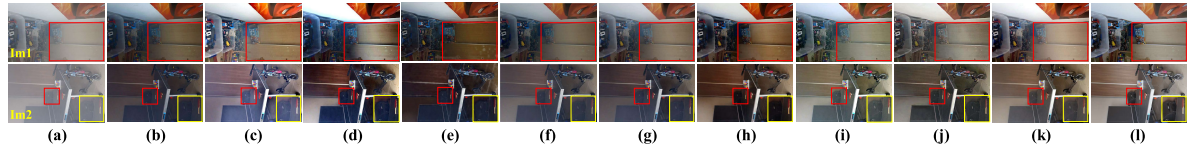
FIGURE 6. Qualitative comparison on I-HAZE. (a) Hazy-Image; (b) DCP [12]; (c) IDE [19]; (d) DDAP [33] (e) SLP [34](f) AOD-Net [20]; (g) DehazeNet [21]; (h) EPDN [25]; (i) TCN [35]; (j) USID-Net [36]; (k) Proposed method; (l) Ground-truth.

where, C_m is the average similarity of the three channels. C_j is the average similarity of a single channel, where $j \in \{1, 2, 3\}$ represents the R, G and B channel. g_i, s_i denotes the total number whose pixel value is i in the ground-truth image and the dehazed image, respectively. N is the number of pixel values (0-255) and Z is 3.

A hundred images were randomly selected from the SOTS dataset, and Eq. (23) was applied to calculate their average histogram similarity, as shown in Fig. 3. The red box shows that our results achieved the highest score of 0.7710, which is 0.1389 higher than the second ranked GCANet [26]. Additionally, the proposed dehazing method produces better visual effects. It has thus been empirically demonstrated that introducing the scattering compensation coefficient into the atmospheric light term of the classical ASM effectively prevents color cast artifacts.

C. QUALITATIVE COMPARISON ON SYNTHETIC DATASETS

We compared IDACC with other SOTA methods on the RESIDE [37] dataset. Although most methods achieve good visual results, as shown in Figs. 4 and 5, there still exist prevalent challenges within the dehazing outcomes, which include color cast, haze residue, low brightness, and loss of details. The dehazing results of DCP [12], IDE [19], AOD-Net [20], DehazeNet [21], EPDN [25], TCN [35] and DDAP [33] exist with different degrees of color cast (see Im1-Im4 and Im6 in Fig. 4(b) and (g); Im1-Im3 in Fig. 4(d); and Im1 in Fig. 5(b), (e), (f) and (g)). Moreover, the dehazed images of DCP, AOD-Net, DDAP and EPDN are generally low brightness. Furthermore, the dehazing results of IDE and AOD-Net achieved good visual results; however, their recovered results are too bright and a have haze residue, respectively (see Im1 in Fig. 5(d)). Although DehazeNet and USID-Net show better visual results compared with other methods, they involve loss of detail and color cast, respectively (see Im2 in Fig. 4(e); and Im8 in 4 (h)). Compared with SOTA methods, experimental results demonstrate that our dehazing results achieved the best visual result, avoiding color cast, low brightness, haze residue, and loss of details (see Figs. 4(i) and 5(i)). Moreover, these experimental

findings demonstrate that our results are the best because the dehazing images are the closest to ground-truth images, which agree with the hazy-free images in the real scenes that people see. Conclusively, our method achieved the best visual results because we altered the atmospheric light term of the traditional ASM by introducing the scattering compensation coefficient, which suppressed the occurrence of color cast. Benefiting from NASM, we also avoided haze residue, low brightness, and loss of details.

D. QUALITATIVE COMPARISON ON REAL-WORLD DATASETS

To comprehensively evaluate and prove the superiority of our method, the I-HAZE [38] and O-HAZE [39] datasets that had relatively dense haze were used in our experiments. Fig. 6 shows that DCP [12], IDE [19], AOD-Net [20], DehazeNet [21], EPDN [25], and DDAP [33] are more effective in processing indoor hazy images, but these methods recovered results that had color cast, low brightness, too bright, and haze residue. In Fig. 7, DCP, IDE, AOD-Net, DehazeNet, and DDAP methods have limited ability to remove haze for scenes with dense haze. Moreover, the results had a large amount of haze residue and different degrees of color cast. Although EPDN and USID-Net [36] have a stronger ability to remove dense haze, the dehazed results have color cast and low brightness. We conducted experiments on hazy images from the Internet. As Fig. 8 shows DCP, AOD-Net, DehazeNet, EPDN, TCN and DDAP were low brightness. Although IDE and USID-Net solve the problem of dullness, its recovered results contain color cast and contrast reduction. This is similar to DCP, AOD-Net, DehazeNet, EPDN and DDAP (see Im2 in Fig. 8(b) and Figs. 8 ((d)-(h))). In comparison, as we can see in Figs. 6(i), 7(i), and 8(j), the proposed method achieved the best visual results on real-world hazy images. This is due to two reasons. First, we used IDACC for image dehazing, and our method required no prior knowledge, thus avoiding the uncertainty caused by applying prior knowledge to all real scenes. Second, our IDACC is different from the learning-based methods, which optimize parameters from the training
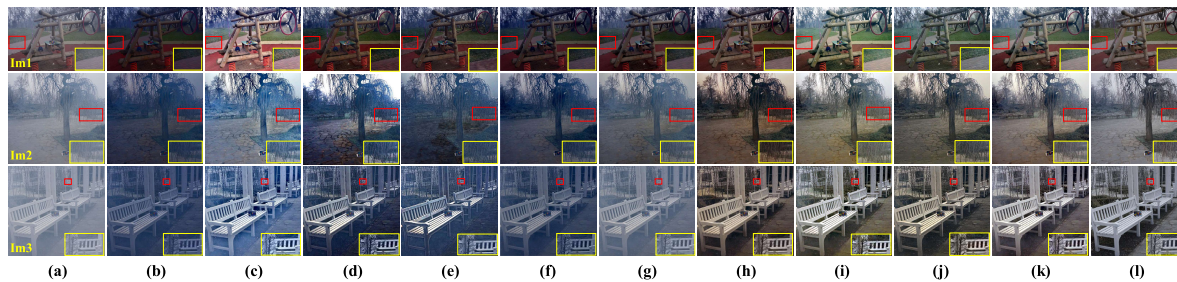
FIGURE 7. Qualitative comparison on O-HAZE. (a) Hazy-Image; (b) DCP [12]; (c) IDE [19]; (d) DDAP [33] (e) SLP [34](f) AOD-Net [20]; (g) DehazeNet [21]; (h) EPDN [25]; (i) TCN [35]; (j) USID-Net [36]; (k) Proposed method; (l) Ground-truth.
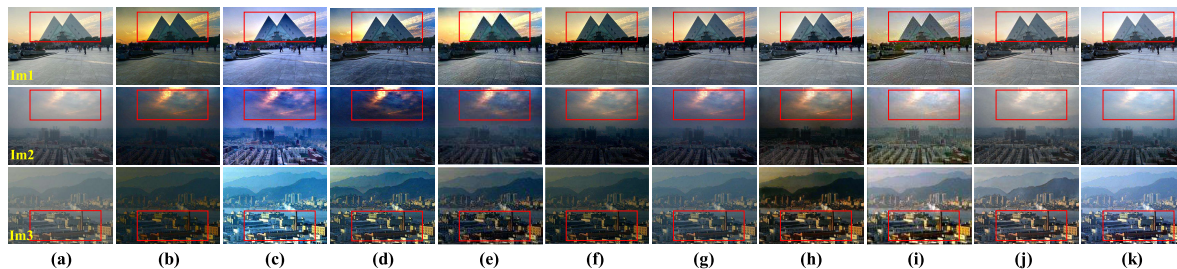

FIGURE 8. Qualitative comparison on real-world. (a) Hazy-Image; (b) DCP [12]; (c) IDE [19]; (d) DDAP [33] (e) SLP [34](f) AOD-Net [20]; (g) DehazeNet [21]; (h) EPDN [25]; (i) TCN [35]; (j) USID-Net [36]; (k) Proposed method.

TABLE 1. Quantitative comparison on SOTS dataset. The recovered images shown in Fig. 4. The best, and second best performances are shown by red and blue, respectively.

Type	Methods	Metrics	Im1	Im2	Im3	Im4	Im5	Im6	Im7	Im8
Learning-based methods	DehazeNet	PSNR	26.8829	28.1003	21.5827	19.1274	18.9004	18.0657	25.0796	16.7433
		SSIM	0.7918	0.9652	0.8565	0.9082	0.8631	0.8415	0.8931	0.8909
	AOD-Net	PSNR	16.6046	18.7556	18.5738	19.1441	18.0372	17.2239	21.6311	17.6925
		SSIM	0.7756	0.8901	0.8622	0.9115	0.8874	0.8824	0.9192	0.8808
	EPDN	PSNR	21.3984	20.7353	21.2345	15.1969	20.6211	14.5305	24.3772	21.1338
		SSIM	0.8926	0.8910	0.8935	0.8015	0.8955	0.8065	0.9266	0.9442
	TCN	PSNR	19.2984	20.0189	20.5845	20.6001	21.5856	21.8272	20.5301	18.6857
		SSIM	0.8441	0.9438	0.8964	0.9421	0.8850	0.8819	0.9028	0.8897
	USID-Net	PSNR	26.3410	25.9062	23.7311	23.6530	26.6588	26.9363	22.8520	20.5322
		SSIM	0.9248	0.9101	0.8349	0.8638	0.8915	0.8679	0.7563	0.5022
ASM-based methods	DCP	PSNR	15.8561	15.4761	15.7579	14.6871	14.7104	13.5901	18.0806	12.2798
		SSIM	0.8213	0.7816	0.7295	0.7840	0.7637	0.7690	0.8735	0.7471
	IDE	PSNR	13.0157	16.7693	15.1436	17.2729	14.4678	13.5376	14.9109	17.1124
		SSIM	0.7118	0.8555	0.7768	0.8623	0.7234	0.7169	0.8095	0.8777
	DDAP	PSNR	14.3029	16.3202	17.8861	14.2800	12.5901	12.0224	19.3138	13.0279
		SSIM	0.7714	0.8087	0.8492	0.7977	0.7102	0.7478	0.9166	0.7321
	SLP	PSNR	19.1757	14.0168	23.7678	15.7531	14.0828	12.9745	20.6667	13.9702
		SSIM	0.9330	0.8438	0.9317	0.8819	0.7957	0.8051	0.9104	0.8248
	Proposed method	PSNR	31.7585	33.1600	32.9852	32.9197	35.6847	32.1105	22.1598	22.3002
		SSIM	0.9436	0.9822	0.9320	0.9764	0.9720	0.9537	0.9092	0.7916

TABLE 2. Quantitative comparison on SOTS dataset. The best, and second best performances are shown by red and blue, respectively.

Metrics	Learning-based methods					ASM-based methods				
	AOD-Net	DehazeNet	EPDN	TCN	USID-Net	DCP	IDE	DDAP	SLP	Proposed method
PSNR	19.9074	22.7852	21.7787	19.7106	23.6563	16.7439	15.2423	16.6087	20.4505	27.5852
SSIM	0.8877	0.8828	0.8846	0.8667	0.7580	0.8211	0.7861	0.8184	0.8986	0.9143

datasets during training; however, these learned parameters do not apply to all real-world hazy images. This causes the performance of the learning-based methods to degrade when processing real-world hazy images. Compared with SOTA

methods, IDACC needs to only input a hazy image and can directly output a high-quality haze-free image, improving the efficiency of image dehazing. The experimental results demonstrate that IDACC achieves the best visual results and

TABLE 3. Quantitative comparison on Hsts dataset. The best, and second best performances are shown by red and blue, respectively.

Metrics	Learning-based methods					ASM-based methods				Proposed method
	AOD-Net	DehazeNet	EPDN	TCN	USID-Net	DCP	IDE	DDAP	SLP	
PSNR	19.6248	23.9865	21.6899	19.8509	23.6563	17.3851	15.2640	17.0170	19.2730	23.5472
SSIM	0.8532	0.8877	0.8826	0.8380	0.7580	0.7928	0.7179	0.7933	0.8313	0.8470

TABLE 4. Quantitative comparison on I-haze dataset. The best, and second best performances are shown by red and blue, respectively.

Metrics	Learning-based methods					ASM-based methods				Proposed method
	AOD-Net	DehazeNet	EPDN	TCN	USID-Net	DCP	IDE	DDAP	SLP	
PSNR	14.7656	15.2539	15.0088	16.5000	16.3630	13.2250	14.7356	14.0588	13.2485	15.4680
SSIM	0.5616	0.5627	0.5664	0.7269	0.5538	0.5121	0.4843	0.5181	0.6484	0.5904

TABLE 5. Quantitative comparison on O-haze dataset. The recovered images shown in Fig. 7. The best, and second best performances are shown by red and blue, respectively.

Type	Methods	Metrics	Im1	Im2	Im3
Learning-based methods	AOD-Net	PSNR	16.1672	14.4144	15.5549
		SSIM	0.6040	0.5624	0.5244
	DehazeNet	PSNR	18.8253	17.6190	17.0370
		SSIM	0.7026	0.6761	0.5955
	EPDN	PSNR	21.4215	15.2866	18.7069
		SSIM	0.8175	0.4837	0.4072
	TCN	PSNR	17.0655	21.0663	19.7216
		SSIM	0.7591	0.7868	0.7172
	USID-Net	PSNR	22.5120	17.8345	16.9756
		SSIM	0.6770	0.5698	0.3409
ASM-based methods	DCP	PSNR	14.9276	12.9731	14.6969
		SSIM	0.5270	0.4717	0.4404
	IDE	PSNR	14.1073	16.3981	16.4769
		SSIM	0.6126	0.5858	0.5061
	DDAP	PSNR	17.3986	15.2267	15.4942
		SSIM	0.6896	0.5714	0.5700
	SLP	PSNR	18.2718	13.8597	15.2076
		SSIM	0.7386	0.6270	0.5752
	Proposed method	PSNR	21.1558	20.9266	20.4207
		SSIM	0.7660	0.6483	0.6254

the dehazed results are the closest to real images, avoiding color cast, low brightness, haze residue, and loss of details.

E. QUANTITATIVE COMPARISON WITH SOTA METHODS

Tables 1 and 2 show scores of different dehazing methods on the SOTS dataset, and Table 1 shows the scores of the recovered images of different dehazing methods in Fig. 4. From Table 1, our method achieved the highest scores in PSNR and SSIM, indicating that our dehazed images are closest to ground-truth images (see Fig. 4(i)). Table 2 shows the average values of PSNR and SSIM scores for different dehazing methods on the SOTS dataset. Here, our method achieved the highest PSNR and SSIM scores of 27.5852 dB and 0.9143, respectively. Additionally, PSNR scores are 3.9289 dB higher than USID-Net [36], which is ranked second, and our SSIM scores are 0.0266 higher than AOD-Net [20], which is ranked second. According to Table 3, the results on the HSTS dataset are closer to the best method than other ASM-based methods. We also experimented on I-HAZE [38] and O-HAZE [39] datasets to comprehensively evaluate the dehazing performance of our method, as shown in Table 4 and Table 5, respectively. Our method obtained the third best PSNR and SSIM scores in Table 4 and the dehazing

results in Fig. 6. Although it is not the highest PSNR and SSIM in Im1 of Fig. 7, the color of our dehazed result is closest to ground-truth images in real scenes. In general, the visual result of our method is better in Fig. 7.

From the aforementioned results, we can conclude the following. First, our method does not rely on prior knowledge, which is significantly superior to existing prior-based methods. Second, our method is more efficient than learning-based methods in image dehazing because it does not consume time for dataset collection and model training. Third, although some PSNR and SSIM scores of the dehazing results from our method are not the highest, they also perform well in image dehazing, avoiding color cast, detail preservation, and producing restored images closest to the ground-truth images. Fourth, our method, however, is not without some limitations. Compared with indoor image dehazing, our method works better in outdoor situations.

VI. CONCLUSION

In conclusion, we obtained the NASM by introducing a scattering compensation coefficient into the atmospheric light term of the traditional ASM. NASM major advantage is that it avoids color cast in dehazed images. Furthermore, we proposed the IDACC algorithm that uses NASM for image dehazing. Moreover, to facilitate the calculation of the transmission map, we designed a GIS based on the minimum value channel. Note that the proposed method needs no training process, thereby ensuring the efficiency of the algorithm. Extensive experiments show that the IDACC algorithm effectively implements hazy image dehazing and avoids color cast. Qualitative and quantitative experiments demonstrate that IDACC outperforms other SOTA dehazing methods.

Regarding future work, we will further refine the approximation parameters in the proposed IDACC. Moreover, the proposed NASM should be extended to combine with deep learning to develop better defogging methods.

REFERENCES
[1] R. Cong, J. Lei, H. Fu, M.-M. Cheng, W. Lin, and Q. Huang, "Review of visual saliency detection with comprehensive information," *IEEE Trans. Circuits Syst. Video Technol.*, vol. 29, no. 10, pp. 2941–2959, Oct. 2019.

[2] T. Sun, Z. Li, X. Xiao, Z. Guo, W. Ning, and T. Ding, "Cascaded detection method for surface defects of lead frame based on high-resolution detection images," *J. Manuf. Syst.*, vol. 72, pp. 180–195, Feb. 2024.

[3] N. Carion, F. Massa, G. Synnaeve, N. Usunier, A. Kirillov, and S. Zagoruyko, "End-to-end object detection with transformers," in *Proc. 16th Eur. Conf. Comput. Vis. (ECCV)*, 2020, pp. 213–229.

[4] K. Akita and N. Ukita, "Context-aware region-dependent scale proposals for scale-optimized object detection using super-resolution," *IEEE Access*, vol. 11, pp. 122141–122153, 2023.

[5] M. Liu, H. Pan, H. Ge, and L. Wang, "MS3Net: Multiscale stratified-split symmetric network with quadra-view attention for hyperspectral image classification," *Signal Process.*, vol. 212, Nov. 2023, Art. no. 109153.

[6] C. Sakaridis, D. Dai, S. Hecker, and L. V. Gool, "Model adaptation with synthetic and real data for semantic dense foggy scene understanding," in *Proc. Eur. Conf. Comput. Vis. (ECCV)*, Sep. 2018, pp. 687–704.

[7] C. Sakaridis, D. Dai, and L. Van Gool, "Semantic foggy scene understanding with synthetic data," *Int. J. Comput. Vis.*, vol. 126, no. 9, pp. 973–992, Mar. 2018.

[8] P. Yin, R. Yuan, Y. Cheng, and Q. Wu, "Deep guidance network for biomedical image segmentation," *IEEE Access*, vol. 8, pp. 116106–116116, 2020.

[9] S. K. Nayar and S. G. Narasimhan, "Vision in bad weather," in *Proc. 7th IEEE Int. Conf. Comput. Vis.*, Sep. 1999, pp. 820–827.

[10] R. Fattal, "Single image dehazing," *ACM Trans. Graph.*, vol. 27, no. 3, pp. 1–9, Aug. 2008.

[11] R. T. Tan, "Visibility in bad weather from a single image," in *Proc. IEEE Conf. Comput. Vis. Pattern Recognit.*, Jun. 2008, pp. 1–8.

[12] K. He, J. Sun, and X. Tang, "Single image haze removal using dark channel prior," *IEEE Trans. Pattern Anal. Mach. Intell.*, vol. 33, no. 12, pp. 2341–2353, Dec. 2011.

[13] Q. Zhu, J. Mai, and L. Shao, "A fast single image haze removal algorithm using color attenuation prior," *IEEE Trans. Image Process.*, vol. 24, no. 11, pp. 3522–3533, Nov. 2015.

[14] D. Berman, T. Treibitz, and S. Avidan, "Non-local image dehazing," in *Proc. IEEE Conf. Comput. Vis. Pattern Recognit. (CVPR)*, Jun. 2016, pp. 1674–1682.

[15] C. O. Ancuti and C. Ancuti, "Single image dehazing by multi-scale fusion," *IEEE Trans. Image Process.*, vol. 22, no. 8, pp. 3271–3282, Aug. 2013.

[16] Z. Li and J. Zheng, "Edge-preserving decomposition-based single image haze removal," *IEEE Trans. Image Process.*, vol. 24, no. 12, pp. 5432–5441, Dec. 2015.

[17] W. Wang, X. Yuan, X. Wu, and Y. Liu, "Fast image dehazing method based on linear transformation," *IEEE Trans. Multimedia*, vol. 19, no. 6, pp. 1142–1155, Jun. 2017.

[18] S. C. Agrawal and A. S. Jalal, "Dense haze removal by nonlinear transformation," *IEEE Trans. Circuits Syst. Video Technol.*, vol. 32, no. 2, pp. 593–607, Feb. 2022.

[19] M. Ju, C. Ding, W. Ren, Y. Yang, D. Zhang, and Y. J. Guo, "IDE: Image dehazing and exposure using an enhanced atmospheric scattering model," *IEEE Trans. Image Process.*, vol. 30, pp. 2180–2192, 2021.

[20] B. Li, X. Peng, Z. Wang, J. Xu, and D. Feng, "AOD-net: All-in-one dehazing network," in *Proc. IEEE Int. Conf. Comput. Vis. (ICCV)*, Oct. 2017, pp. 4780–4788.

[21] B. Cai, X. Xu, K. Jia, C. Qing, and D. Tao, "DehazeNet: An end-to-end system for single image haze removal," *IEEE Trans. Image Process.*, vol. 25, no. 11, pp. 5187–5198, Nov. 2016.

[22] W. Ren, S. Liu, H. Zhang, J. Pan, X. Cao, and M.-H. Yang, "Single image dehazing via multi-scale convolutional neural networks," in *Proc. Eur. Conf. Comput. Vis.* Cham, Switzerland: Springer, 2016, pp. 154–169.

[23] B. Li, Y. Gou, J. Z. Liu, H. Zhu, J. T. Zhou, and X. Peng, "Zero-shot image dehazing," *IEEE Trans. Image Process.*, vol. 29, pp. 8457–8466, 2020.

[24] H. Wu, Y. Qu, S. Lin, J. Zhou, R. Qiao, Z. Zhang, Y. Xie, and L. Ma, "Contrastive learning for compact single image dehazing," in *Proc. IEEE/CVF Conf. Comput. Vis. Pattern Recognit. (CVPR)*, Jun. 2021, pp. 10551–10560.

[25] Y. Qu, Y. Chen, J. Huang, and Y. Xie, "Enhanced pix2pix dehazing network," in *Proc. IEEE Conf. Comput. Vis. Pattern Recognit. (CVPR)*, vol. 24, no. 11, pp. 8160–8168, Jun. 2019.

[26] D. Chen, M. He, Q. Fan, J. Liao, L. Zhang, D. Hou, L. Yuan, and G. Hua, "Gated context aggregation network for image dehazing and deraining," in *Proc. IEEE Winter Conf. Appl. Comput. Vis. (WACV)*, 2019, pp. 1375–1383.

[27] X. Xiao, Y. Ren, Z. Li, N. Zhang, and W. Zhou, "Self-supervised zero-shot dehazing network based on dark channel prior," *Frontiers Optoelectron.*, vol. 16, no. 1, p. 7, Apr. 2023.

[28] E. J. McCartney, *Optics of the Atmosphere: Scattering By Molecules and Particles*. New York, NY, USA: Wiley, 1976, p. 421.

[29] S. G. Narasimhan and S. K. Nayar, "Contrast restoration of weather degraded images," *IEEE Trans. Pattern Anal. Mach. Intell.*, vol. 25, no. 6, pp. 713–724, Jun. 2003.

[30] X.-S. Zhang, Y.-B. Yu, K.-F. Yang, and Y.-J. Li, "A fish retina-inspired single image dehazing method," *IEEE Trans. Circuits Syst. Video Technol.*, vol. 32, no. 4, pp. 1875–1888, Apr. 2022.

[31] G. Buchsbaum, "A spatial processor model for object colour perception," *J. Franklin Inst.*, vol. 310, no. 1, pp. 1–26, Jul. 1980.

[32] K. He, J. Sun, and X. Tang, "Guided image filtering," *IEEE Trans. Pattern Anal. Mach. Intell.*, vol. 35, no. 6, pp. 1397–1409, Jun. 2013.

[33] Z. Li, H. Shu, and C. Zheng, "Multi-scale single image dehazing using Laplacian and Gaussian pyramids," *IEEE Trans. Image Process.*, vol. 30, pp. 9270–9279, 2021.

[34] P. Ling, H. Chen, X. Tan, Y. Jin, and E. Chen, "Single image dehazing using saturation line prior," *IEEE Trans. Image Process.*, vol. 32, pp. 3238–3253, 2023.

[35] J. Shin, H. Park, and J. Paik, "Region-based dehazing via dual-supervised triple-convolutional network," *IEEE Trans. Multimedia*, vol. 24, pp. 245–260, 2022.

[36] J. Li, Y. Li, L. Zhuo, L. Kuang and T. Yu, "USID-net: Unsupervised single image dehazing network via disentangled representations," *IEEE Trans. Multimedia*, vol. 25, pp. 3587–3601, 2023.

[37] B. Li, W. Ren, D. Fu, D. Tao, D. Feng, W. Zeng, and Z. Wang, "Benchmarking single-image dehazing and beyond," *IEEE Trans. Image Process.*, vol. 28, no. 1, pp. 492–505, Jan. 2019.

[38] C. Ancuti, C. O. Ancuti, R. Timofte, and C. De Vleeschouwer, "I-HAZE: A dehazing benchmark with real hazy and haze-free indoor images," in *Proc. Int. Conf. Adv. Concepts Intell. Vis. Syst.* Cham, Switzerland: Springer, 2018, pp. 620–631.

[39] C. O. Ancuti, C. Ancuti, R. Timofte, and C. De Vleeschouwer, "O-HAZE: A dehazing benchmark with real hazy and haze-free outdoor images," in *Proc. IEEE/CVF Conf. Comput. Vis. Pattern Recognit. Workshops (CVPRW)*, Jun. 2018, pp. 867–8678.

ZHIWEI LI received the M.S. degree in electronic science and technology from Wuhan University, in 2006, and the Ph.D. degree from Wuhan National Laboratory for Optoelectronics, Huazhong University of Science and Technology, in 2016. He is currently an Associate Professor with Shanghai Technology and Innovation Vocational College. His research interests include intelligent theory and control, image processing, and optoelectronics.

XINJIE XIAO received the M.E. degree from the School of Electronic and Electrical Engineering, Shanghai University of Engineering Science, Shanghai, China, in 2023. He is currently pursuing the Ph.D. degree in control science and engineering with Donghua University, Shanghai. His current research interests include deep learning and image processing.

NANNAN ZHANG received the M.E. degree from the School of Electronic and Electrical Engineering, Shanghai University of Engineering Science, Shanghai, China, in 2023. He is currently focusing on deep learning and image processing. His research interests include machine learning and computer vision.